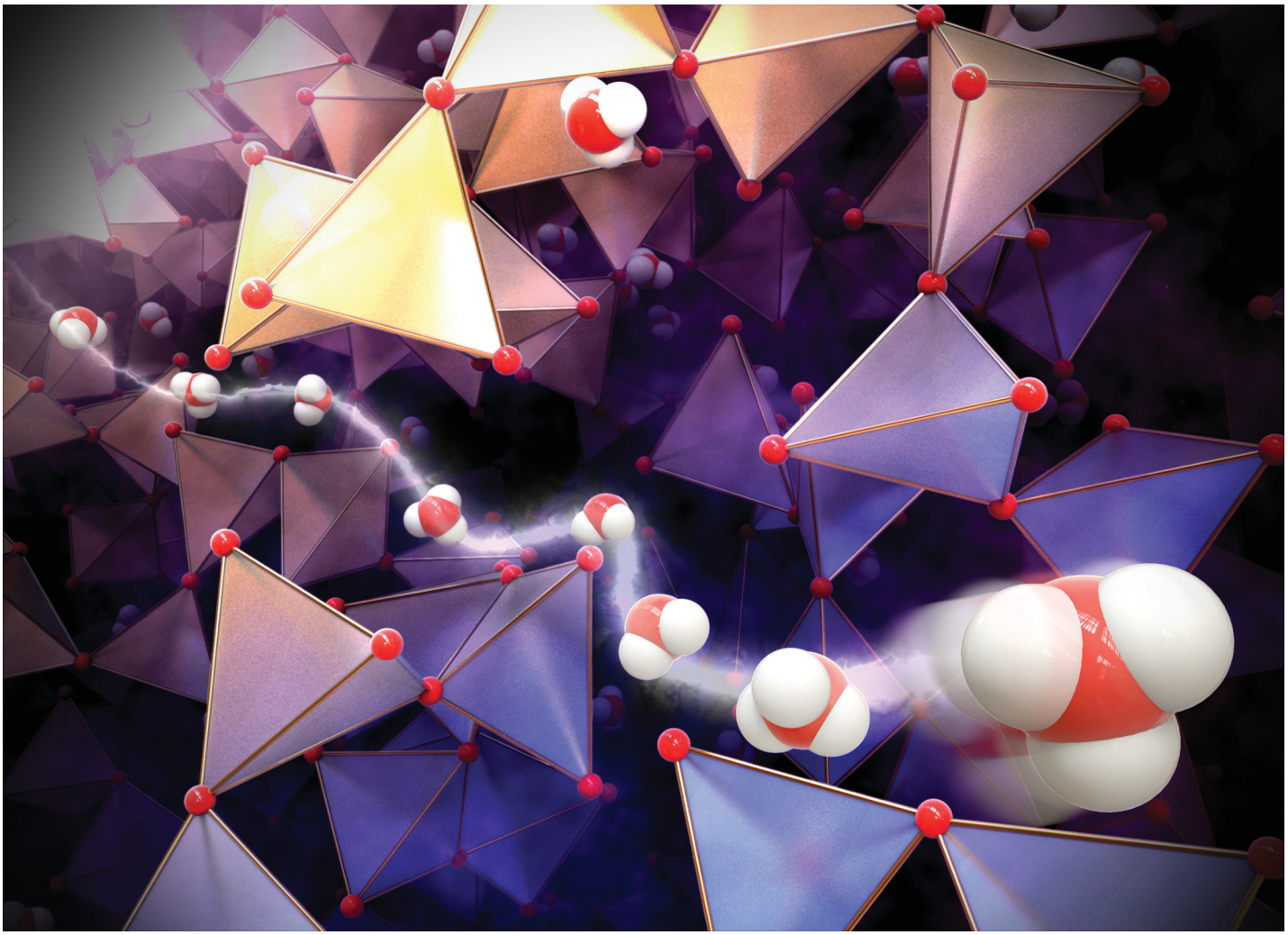

Showcasing research from Lecturer Yasuaki Matsuda's laboratory, Department of Applied Chemistry, Osaka Institute of Technology, Osaka, Japan.

High proton conductivity of $NaMg_{1-x}Li_xH_x(PO_3)_3{\cdot}yH_2O$ with a three-dimensional open framework in the intermediate temperature range

A mixed cation phosphate, $NaMg_{1-x}Li_xH_x(PO_3)_3{\cdot}yH_2O$ with a three-dimensional tunnel structure exhibited high proton conductivity over 10^{-2} S cm^{-1} by diffusion of H_3O^+ along the PO_4 tetrahedral chain in the tunnel in the wide temperature range of 150–500°C under a non-humidified atmosphere.

As featured in:

See Yasuaki Matsuda *et al.*, *Mater. Adv.*, 2021, **2**, 6603.

ROYAL SOCIETY OF CHEMISTRY

rsc.li/materials-advances

Registered charity number: 207890

Materials Advances

ROYAL SOCIETY OF CHEMISTRY

PAPER

View Article Online
View Journal | View Issue

Cite this: *Mater. Adv.*, 2021, 2, 6603

High proton conductivity of $NaMg_{1-x}Li_xH_x(PO_3)_3 \cdot yH_2O$ with a three-dimensional open framework in the intermediate temperature range†

Naoya Ueda,[a] Jun Nakajima,[a] Daisuke Mori,[b] Sou Taminato,[b] Nobuyuki Imanishi,[b] Shinya Higashimoto[a] and Yasuaki Matsuda *[a]

Proton solid electrolytes, which exhibit high proton conductivity and thermal stability in a wide range of intermediate temperatures, are desirable for operating fuel cells at a temperature suitable for applications such as automobiles and cogeneration systems. A new proton conductor $NaMg_{1-x}Li_xH_x(PO_3)_3 \cdot yH_2O$ was synthesised by a coprecipitation method. Powder X-ray structure refinement reveals that the three-dimensional tunnel framework is formed by the sharing of corner oxygens of zigzag PO_4 tetrahedral chains and face-shared $(NaO_6)(MgO_6)$ chains. In the three-dimensional tunnel, the oxygen sites of water for crystallisation were observed. In Fourier transform infrared spectroscopy (FTIR) measurement, an increase in absorption peaks corresponding to the modes of O–H and P–O–H bonds for x in $NaMg_{1-x}Li_xH_x(PO_3)_3 \cdot yH_2O$ was observed, which reflects the introduction of protons to the crystal structure. Although a multi-step weight loss due to desorption of water of crystallisation was observed for thermogravimetry (TG) curves, $NaMg_{1-x}Li_xH_x(PO_3)_3 \cdot yH_2O$ retained the framework up to 800 °C. The proton conductivity shows a positive tendency for x. $NaMg_{0.8}Li_{0.2}H_{0.2}(PO_3)_3 \cdot yH_2O$ exhibited a high proton conductivity of over 10^{-2} S cm^{-1} in the temperature range of 150–500 °C, and the value reached 2.4×10^{-2} S cm^{-1} at 225 °C under a non-humidified atmosphere. The proton conductivity of $NaMg_{0.8}Li_{0.2}H_{0.2}(PO_3)_3 \cdot yH_2O$ changed with the amount of crystalline water. In a humidified atmosphere (p_{H_2O} = 4 kPa), $NaMg_{0.8}Li_{0.2}H_{0.2}(PO_3)_3 \cdot yH_2O$ exhibited a conductivity of over 10^{-3} S cm^{-1} from room temperature to 500 °C and reached 2.6×10^{-2} S cm^{-1} at 225 °C. After keeping the dehydrated sample in the humidified atmosphere at room temperature for 2 h, $NaMg_{0.8}Li_{0.2}H_{0.2}(PO_3)_3 \cdot yH_2O$ showed a proton conductivity of over 10^{-2} S cm^{-1} again in the intermediate temperature range.

Received 9th July 2021,
Accepted 8th August 2021

DOI: 10.1039/d1ma00592h

rsc.li/materials-advances

Introduction

Proton conduction is a common phenomenon observed in various materials, including liquids and organic and inorganic solids,[1–6] and is essential for the metabolism of biological systems[7–9] and the operation of fuel cells.[10–12] In particular, proton conductors are important for practical applications as electrolytes that determine the operating temperature of fuel cells. Since the chemical reaction rate is thermally excited and the selectivity of the reactions is excellent at a low temperature, the operating temperature of the fuel cells is desirable in the temperature range of 100–500 °C. Acids, liquid-impregnated polymers,[1] metal–organic framework (MOF) systems,[2,12–14] and inorganic solids such as $CsHSO_4$ and CsH_2PO_4[3,15–17] exhibit high proton conductivity below low-intermediate temperatures. In-doped SnP_2O_7 exhibits a high proton conductivity up to 350 °C.[4,11] Perovskites exhibit excellent thermal stability and high proton conductivity above 300 °C.[5,6,18,19] Although all of them are excellent proton conductors, they have a common issue that they exhibit high proton conductivity in a limited temperature range.

To develop materials that exhibit thermal stability and high proton conductivity, it is necessary to find a new structure with a proton diffusion pathway in the inorganic framework. In developing such materials, the material design that divides the structure into inorganic blocks and hydrogen bond networks observed in MOF-based materials is considered attractive. However, the use of non-combustible inorganic blocks is not sufficient, and a framework formed only by strong bonds, such as covalent and ionic bonds like perovskites, is needed to achieve thermal stability above 500 °C. Furthermore, to develop high proton conductivity, it needs to form a hydrogen bond network that results in the proton conduction pathway by

[a] *Department of Applied Chemistry, Faculty of Engineering, Osaka Institute of Technology, 5-16-1 Ohmiya, Asahi-Ku, Osaka, 535-8585, Japan. E-mail: yasuaki.matsuda@oit.ac.jp*
[b] *Department of Chemistry for Materials, Graduate School of Engineering, Mie University, Tsu, Mie 514-8507, Japan*

† Electronic supplementary information (ESI) available. See DOI: 10.1039/d1ma00592h

controlling the arrangement of molecules, and retention of these molecules up to intermediate temperatures.

Mixed cation phosphates are attractive materials that exhibit high proton conductivity in a wide temperature range. $AMg_{1-x}H_{2x}(PO_3)_3{\cdot}yH_2O$ (A: Rb^+ and K^+) has a one-dimensional tunnel framework that is composed of face-shared $(AO_6)(MgO_6)$ chains and PO_4 chains.[20,21] Water molecules were arranged along the PO_4 chains *via* hydrogen bonds in the tunnel and retained by the connection *via* a coordination bond with a large alkali cation that forms the framework. Although a phase transition occurs at around 300 °C, these tunnel phosphates exhibit a high proton conductivity of over 10^{-3} S cm^{-1} from room temperature to 250 °C. Benitoite-type phosphate, which is the high-temperature phase of $KMg_{1-x}H_{2x}(PO_3)_3{\cdot}yH_2O$, has a layered framework formed by stacking the layers of the edge-shared $(AO_6)(MgO_6)$ octahedral units and those of the P_3O_9 ring in the *c*-axis direction, and exhibits a high proton conductivity up to 500 °C.[22]

Mixed cation phosphates form various open frameworks by combining cations with different valences, sizes, and synthesis conditions.[20–25] These open frameworks are formed by a rigid connection between the octahedral cations and PO_4 tetrahedra, which results in the thermal stability of the proton conductors. Since the PO_4 tetrahedra tend to form hydrogen bonds, the connection of the PO_4 tetrahedra provides an adjacent arrangement of water molecules in the tunnel framework, which participates as a proton conduction pathway. Water molecules that exist in the tunnel are not only connected to the PO_4 tetrahedra *via* hydrogen bonds, but their oxygen also coordinates with large alkaline cations.[21] Furthermore, with mixed cation phosphate, proton conductivity is expected to improve with the introduction of protons as charge compensation for the formation of cation deficiency and the substitution of aliovalent cations. The phase transition of $KMg_{1-x}H_{2x}(PO_3)_3{\cdot}yH_2O$ is thought to occur to extend the distance between the alternately arranged K^+ and Mg^+. Although it is desirable to include a large cation for the formation of coordination bonds with oxygen in water molecules, it is necessary to select cations smaller than K^+ to prevent the phase transition. In the present study, we focus on $NaMg(PO_3)_3$, which has a three-dimensional open framework with PO_4 chains.[26] Improvement of proton conductivity was attempted by introducing protons into $NaMg_{1-x}Li_xH_x(PO_3)_3{\cdot}yH_2O$. To introduce protons as charge compensation of aliovalent substitution, $NaMg_{1-x}Li_xH_x(PO_3)_3{\cdot}yH_2O$ was synthesised with a coprecipitation method and revealed the exhibition of a proton conductivity exceeding 10^{-2} S cm^{-1} in a wide temperature range of 150–500 °C without large humidification. This paper discusses the relationship among the composition, structure, and proton conductivity of $NaMg_{1-x}Li_xH_x(PO_3)_3{\cdot}yH_2O$.

Experimental

The $NaMg_{1-x}Li_xH_x(PO_3)_3{\cdot}yH_2O$ series was synthesised by the coprecipitation method. Appropriate molar ratios of Na_2CO_3 (Nacalai Tesque, >99.5%), Li_2CO_3 (Wako) and $(MgCO_3)_4Mg(OH)_2{\cdot}xH_2O$ (Nacalai Tesque) were weighed and dissolved in 30 mL of phosphoric acid solution (0.5 mol L^{-1}, Kanto Chemical Lab. Co.). The solution was heated at 120 °C in air for a day, and a white-coloured residual powder was obtained. The sample powder obtained was pressed into a pellet (10 mm diameter, 1–2 mm thick) and then heated in air at 400 °C for 12 h on an alumina boat with an intermediate grinding step. X-ray diffraction (XRD) patterns for the powder samples were obtained using a diffractometer (Rigaku RINT2000) with CuKα radiation in the 2θ range from 10° to 90° with 0.02 step widths. Thermogravimetry/differential thermal analysis (TG/DTA; Rigaku Thermo Plus EVO TG 8120) was performed at a heating rate of 10 °C min^{-1} under a N_2 gas flow. The structures of the samples were refined by X-ray Rietveld analysis using the Z-Rietveld programme.[27] The activation energy was estimated using the soft VB programme.[28] Fourier transform infrared (FTIR) absorption spectra of the samples were recorded with an IR Affinity 1S spectrometer (Shimadzu Inc.) with a spectral range of 600–4000 cm^{-1}, 50 scans and a resolution of 0.5 cm^{-1}.

The ionic conductivities were measured by the AC impedance method in the temperature range from room temperature to 500 °C under an N_2 gas flow over the frequency range of 10 Hz to 1 MHz using an LCR metre (Hioki MI3536) as a frequency response analyser. Measurements were performed using a sample pellet (10 mm diameter, 1–2 mm thick) with gold electrodes on each side. The relative density of the measured pellets was approximately 80%.

Results and discussion

$NaMg_{1-x}Li_xH_x(PO_3)_3{\cdot}yH_2O$ was synthesised in order to introduce protons into the crystal as charge compensation by partial substitution of Mg^{2+} with Li^+. Fig. 1 shows the XRD patterns of $NaMg_{1-x}Li_xH_x(PO_3)_3{\cdot}yH_2O$ synthesised in air at 400 °C for 12 h. Diffraction patterns of $NaMg_{1-x}Li_xH_x(PO_3)_3{\cdot}yH_2O$ were similar to those of $NaMg(PO_3)_3$ and all diffraction peaks could be assigned to the space group *Pbca*.[26] The structural parameters of $NaMg_{1-x}Li_xH_x(PO_3)_3{\cdot}yH_2O$ were refined by XRD Rietveld refinement analysis using the structural model (space group

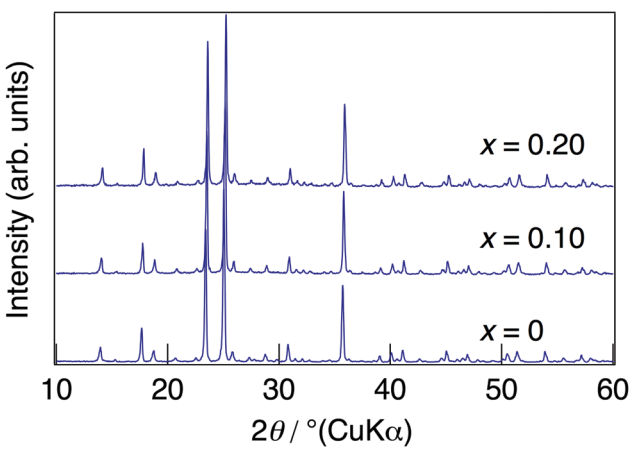

Fig. 1 XRD patterns for $NaMg_{1-x}Li_xH_x(PO_3)_3{\cdot}yH_2O$ synthesised in air at 400 °C for 12 h.

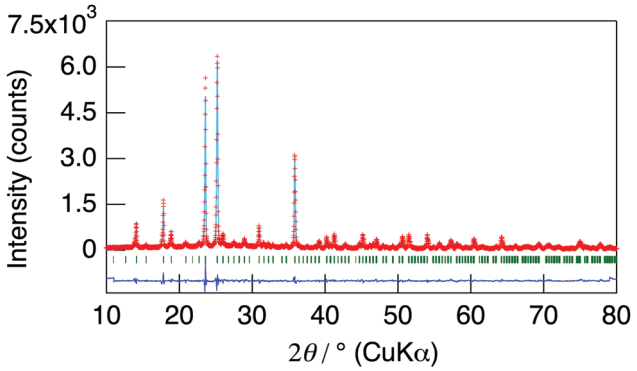

Fig. 2 The observed and calculated XRD patterns and their difference for $NaMg_{1-x}Li_xH_x(PO_3)_3{\cdot}yH_2O$ (x = 0.20).

Pbca).[26] We considered a model in which lithium occupies only Mg1 or Mg2 sites and a model in which lithium occupies both of these sites. The best result was obtained by refinement with the third model. In this model, the lithium occupancy was fixed to the charged composition, and the analysis proceeded. Five oxygen sites in the water of crystallization were newly determined using the differential Fourier synthesis method. Fig. 2 displays the observed and calculated XRD patterns and their difference for $NaMg_{1-x}Li_xH_x(PO_3)_3{\cdot}yH_2O$ (x = 0.20) as representative data. Structural parameters obtained from the final refinement cycle are listed in Table 1. The profile fitting provided good agreement factors; R_{wp} of 10.76%, R_p of 8.31%, R_B of 4.92%, R_F of 4.88%, and S = 1.45.

Fig. 3 presents a change in the refined lattice parameter as a function of x in $NaMg_{1-x}Li_xH_x(PO_3)_3{\cdot}yH_2O$. The a, b, and c axes contracted for x, suggesting the formation of the solid solution in the range of x = 0–0.20. It is thought that the shrinkage of the lattice by the replacement of Li^+ (0.74 Å) with an ionic radius larger than Mg^{2+} (0.72 Å) is caused by the contraction between the oxygens due to the formation of hydrogen bonds with the introduced protons. Fig. 4 depicts the FTIR spectra for $NaMg_{1-x}Li_xH_x(PO_3)_3{\cdot}yH_2O$. To remove the effect of adsorbed water, the samples were dried at 120 °C before measurement. The strong absorbance peaks at 743 cm^{-1} and 970 cm^{-1} can be assigned to the symmetric and asymmetric vibration modes of ν_s(P–O–P) and ν_{as}(P–O–P) stretching vibrations.[23,29] This corresponds to the formation of PO_4 tetrahedral chains. The vibration bands at around 1095 and 1253 cm^{-1} are due to the symmetric and asymmetric PO_2 vibration modes of $\nu_s(PO_2)$, and $\nu_{as}(PO_2)$. The broad absorbance peaks at 2300 and 2750 cm^{-1} are attributed to the vibration modes of ν_s(P–O–H). The ν_s(P–O–H) and ν_{as}(P–O–P) modes in polyphosphates at 684 cm^{-1} and 950 cm^{-1}, respectively, are enhanced by the connection of protons to the PO_4 unit.[29] The bands at approximately 1600 cm^{-1} and 3500 cm^{-1} are assigned to δ (OH) and ν (OH), reflecting the presence of water of crystallisation. These vibration modes reveal strong absorbance peaks with increasing x, which suggests the introduction of H^+ in the crystal structure.

Fig. 5 illustrates the TG/DTA curves for $NaMg_{1-x}Li_xH_x(PO_3)_3{\cdot}yH_2O$ with x = 0 and x = 0.20 measured under an N_2 gas flow

Table 1 Refined structural parameters for $NaMg_{0.80}Li_{0.20}H_{0.20}(PO_3)_3{\cdot}yH_2O$

Atom	Site	g	x	y	z	B/Å^2
P1	8c	1.0	0.020(14)	0.245(15)	0.473(16)	0.5
P2	8c	1.0	0.218(13)	0.225(18)	0.489(16)	0.5
P3	8c	1.0	0.266(13)	0.024(2)	0.481(19)	0.5
P4	8c	1.0	0.275(14)	−0.007(19)	0.267(15)	0.5
P5	8c	1.0	0.474(13)	0.019(2)	0.239(16)	0.5
P6	8c	1.0	0.494(15)	0.233(18)	0.224(18)	0.5
Mg1	8c	0.8	0.122(2)	0.121(3)	0.134(2)	0.5
Li1	8c	0.2	=x(Li1)	=y(Li1)	=z(Li1)	0.5
Mg2	8c	0.8	0.376(2)	0.378(2)	0.380(3)	0.5
Li2	8c	0.2	=x(Li2)	=y(Li2)	=z(Li2)	0.5
Na1	4a	1.0	0	1/2	1/2	0.5
Na2	4b	1.0	1/2	1/2	1/2	0.5
Na3	8c	1.0	0.247(18)	0.251(3)	0.252(2)	0.5
O1	8c	1.0	0.493(3)	0.263(3)	0.126(4)	1.0
O2	8c	1.0	0.04(3)	0.160(3)	0.023(3)	1.0
O3	8c	1.0	0.467(3)	0.327(4)	0.481(4)	1.0
O4	8c	1.0	0.131(3)	0.175(3)	0.442(3)	1.0
O5	8c	1.0	0.224(3)	0.216(4)	0.081(3)	1.0
O6	8c	1.0	0.279(3)	0.273(4)	0.419(4)	1.0
O7	8c	1.0	0.261(3)	0.376(4)	0.019(3)	1.0
O8	8c	1.0	0.157(2)	0.037(3)	0.022(4)	1.0
O9	8c	1.0	0.329(3)	0.474(3)	0.471(3)	1.0
O10	8c	1.0	0.283(2)	0.033(3)	0.356(3)	1.0
O11	8c	1.0	0.228(3)	0.076(3)	0.218(4)	1.0
O12	8c	1.0	0.270(3)	0.397(3)	0.288(3)	1.0
O13	8c	1.0	0.111(3)	0.452(3)	0.241(4)	1.0
O14	8c	1.0	0.475(3)	0.471(3)	0.342(4)	1.0
O15	8c	1.0	0.022(3)	0.038(3)	0.173(3)	1.0
O16	8c	1.0	0.429(2)	0.130(5)	0.198(3)	1.0
O17	8c	1.0	0.414(3)	0.276(4)	0.279(3)	1.0
O18	8c	1.0	0.086(2)	0.203(3)	0.234(3)	1.0
O19	8c	0.60(5)	0.444(4)	0.637(5)	0.769(4)	1.5
O20	8c	0.41(4)	0.876(7)	0.624(8)	0.882(9)	1.5
O21	8c	0.56(5)	0.56(5)	0.392(4)	0.905(5)	1.5
O22	8c	0.23(4)	0.144(10)	0.808(13)	0.202(13)	1.5
O23	8c	0.54(4)	0.166(5)	0.877(4)	−0.032(5)	1.5

Space group: *Pbca* (61), a = 14.239 (3) Å, b = 14.210 (3) Å, c = 14.199 (3) Å, S: 1.45, R_{wp}(%): 10.76, R_p(%): 8.31, R_e(%): 7.40, R_B(%): 4.92, R_F(%): 4.88.

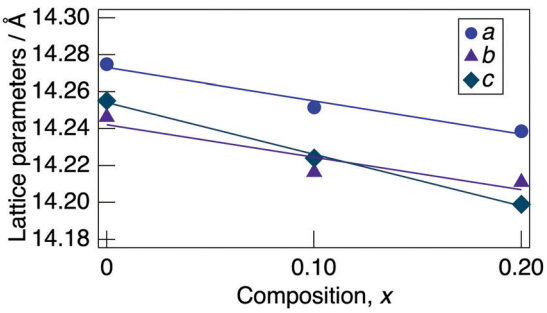

Fig. 3 A change in the refined lattice parameter as a function of x in $NaMg_{1-x}Li_xH_x(PO_3)_3{\cdot}yH_2O$.

with a heating rate of 10 °C min^{-1}. The XRD patterns for $NaMg_{1-x}Li_xH_x(PO_3)_3{\cdot}yH_2O$ (x = 0 and 0.20) measured after holding at different temperatures for 6 h are shown in Fig. S1(a) and (b) (ESI†). For x = 0, a three-step weight loss due to dehydration reactions occurred at room temperature, 150 °C, and 600 °C. For x = 0.20, dehydration reactions were observed at room temperature and 150 °C. The amount of

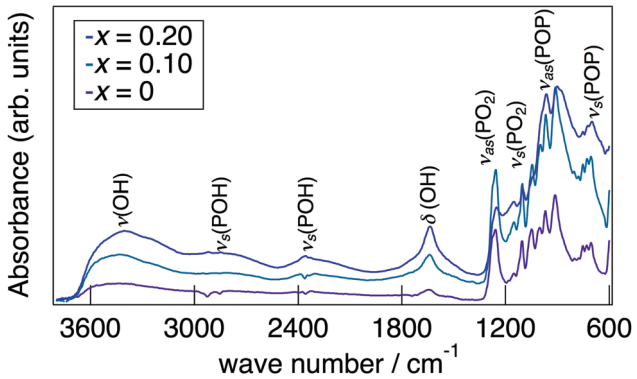

Fig. 4 FTIR spectra of $NaMg_{1-x}Li_xH_x(PO_3)_3{\cdot}yH_2O$.

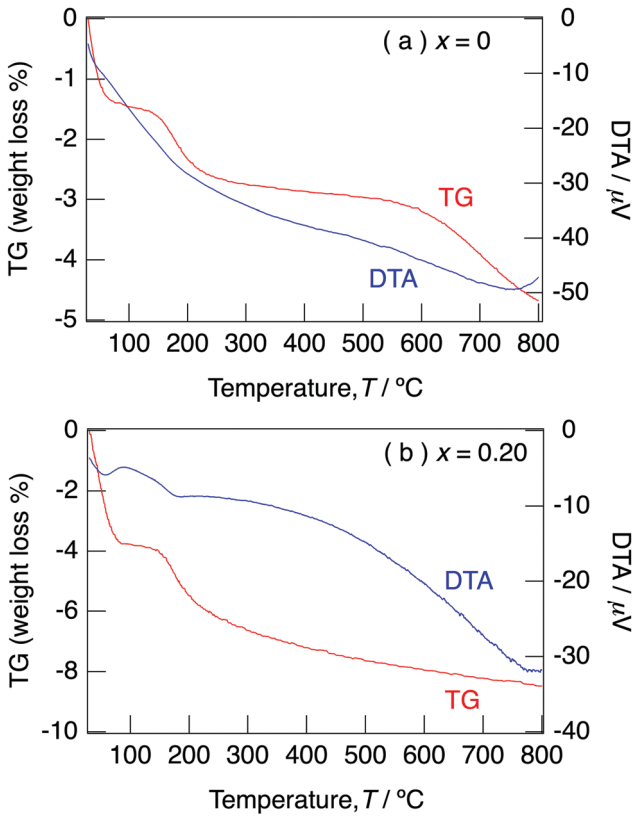

Fig. 5 TG/DTA curves for $NaMg_{1-x}Li_xH_x(PO_3)_3{\cdot}yH_2O$ with x = 0 (a) and x = 0.20 (b) measured under an N_2 gas flow with a heating rate of 10 °C min^{-1}.

weight loss for the temperature of the samples with x = 0.20 decreased from 250 °C, and a dehydration reaction proceeded up to 800 °C. No impurity peaks were observed for XRD patterns for the samples with x = 0–0.20 and the framework was retained up to 800 °C. It is considered that the water of crystallisation desorbed at 600 °C for the sample with x = 0 and desorbed at 250 °C due to the introduction of H^+ for the samples with x = 0.20. The oxygens of water molecules coordinate with cations using their lone pairs; therefore, the formation of H_3O^+ due to the connection of H^+ and lone pairs weakens the coordination

Table 2 Water contents of $NaMg_{1-x}Li_xH_x(PO_3)_3{\cdot}yH_2O$ calculated from the weight loss in the range of 30–800 °C

x	0	0.10	0.20
Water content	0.7	1.1	1.2

bonding of water molecules. The initial weight loss corresponds to the loss of adsorbed water and water of crystallisation, and the second step corresponds to the loss of only water of crystallisation. Water contents of $NaMg_{1-x}Li_xH_x(PO_3)_3{\cdot}yH_2O$, as calculated from the weight loss in the range of 30–800 °C, are summarised in Table 2. The water content of the samples tended to increase with x and varied from 0.7 to 1.2 per unit formula.

Fig. 6 presents the crystal structure of $NaMg_{0.8}Li_{0.2}H_{0.2}(PO_3)_3{\cdot}yH_2O$ viewed along the [001] direction (a) and PO_4 chains along the a-axis direction with oxygens of water molecules adjacent to PO_4 tetrahedra (b). The averaged bond length and bond angles of $NaMg_{1-x}Li_xH_x(PO_3)_3{\cdot}yH_2O$ are summarised in Table S1 (ESI†). Sodium ions are shown in light blue spheres, magnesium ions are yellow ones, and PO_4 tetrahedra are displayed in dark gray in the figure. The newly detected oxygens of the water molecule are indicated by dark blue spheres. The PO_4 tetrahedra are connected by the sharing of corner oxygens to form a zigzag chain along the a-axis direction. Face-shared $(NaO_6)(MgO_6)$ octahedral chains are linked along the [111] direction, and crystallographically equivalent octahedral chains are connected by corner-sharing with the zigzag PO_4 chains to form a three-dimensional open framework. Two of the oxygens in the PO_4 tetrahedron are shared by the NaO_6 and MgO_6 octahedra, and the others connect with the adjacent PO_4 tetrahedra. One of the P–O bonds shared by adjacent PO_4 was longer than the others, and these values varied in the range of 1.39–1.96 Å. The bond angles of O–P–O ranged from 92–130° and were distorted from the ideal tetrahedral bond angle of 109.5°. No systematic changes in the bond length or bond angle for compositional changes were observed for cations composing the framework.

Five oxygens of the water molecules exist in the three-dimensional tunnel along with PO_4 tetrahedral chains. The enhancement of the P–O–H and P–O–P absorption peaks for x in the FTIR spectra reflects the formation of O–H bonds between protons and oxygens of the PO_4 tetrahedra. Since water molecules are connected to the PO_4 tetrahedron *via* hydrogen bonds, they are thought to be arranged adjacent to the PO_4 tetrahedral chain. Three oxygens, O21–23, form bonds with Na^+ in the range of 1.9–2.45 Å and exist as coordination water molecules, which would be due to the preference of large cations for a large coordination number of anions.[21]

The rigid framework formed by covalent and/or ionic bonds without the connection of hydrogen bonds with molecules results in the retention of the structure up to 800 °C, even if the desorption of water of crystallisation occurs. The weight loss due to the stepwise dehydration reaction on the TG curves comes from the different coordination environments of the water molecules in the tunnel. Coordinated water molecules

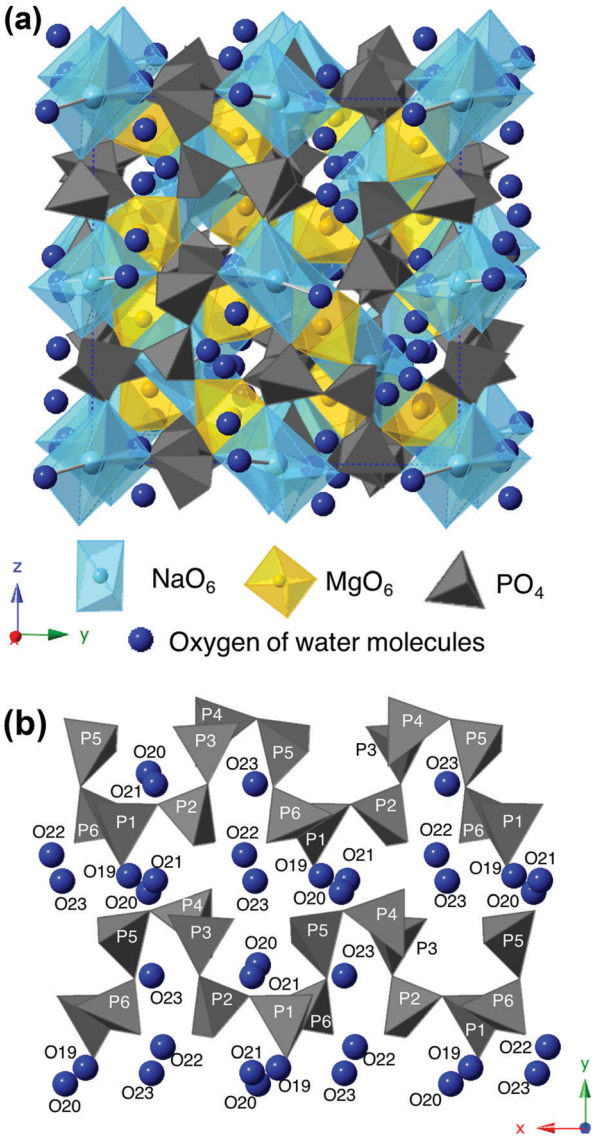

Fig. 6 The crystal structure of $NaMg_{0.8}Li_{0.2}H_{0.2}(PO_3)_3{\cdot}yH_2O$ viewed along the [001] direction (a) and PO_4 chains along the *a*-axis direction with oxygens of water molecules (b).

connected with Na^+ should be maintained up to high temperatures.[21] It is thought that the formation of H_3O^+ would weaken the contact between Na^+ and water molecules; however, a TG curve of $x = 0.20$ suggests residual water of crystallisation above 500 °C. This material has the potential for exhibiting high proton conductivity up to intermediate temperatures due to the proton diffusion accompanied by the hopping of water molecules in the tunnel along PO_4 chains.[20,21]

Fig. 7 depicts the Cole–Cole plots for the sample with $x = 0.20$ in $NaMg_{1-x}Li_xH_x(PO_3)_3{\cdot}yH_2O$ measured at different temperatures under a non-humidified N_2 gas flow. The plots for the samples with $x = 0.20$ showed a spike due to the electrode contribution, which is a typical behaviour for materials with high ionic conductivity. The total resistivity was obtained from the real axis intercepts of the spike caused by the electrode

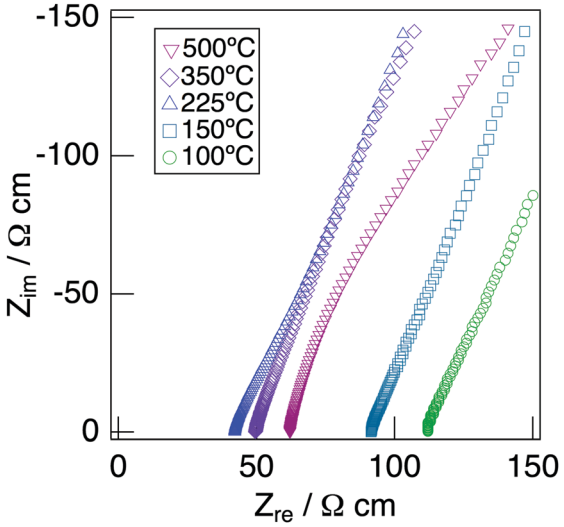

Fig. 7 Cole–Cole plots for the sample with $x = 0.20$ in $NaMg_{1-x}Li_xH_x(PO_3)_3{\cdot}yH_2O$ measured at different temperatures under a non-humidified N_2 gas flow.

contribution. The conductivity increased up to 225 °C and then decreased, which would be due to the dehydration. Fig. 8 shows the temperature dependence of the proton conductivity of $NaMg_{1-x}Li_xH_x(PO_3)_3{\cdot}yH_2O$ measured under a non-humidified N_2 gas flow. The proton conductivity increased with *x*, reflecting the introduction of protons. The conductivity of $x = 0$ increased

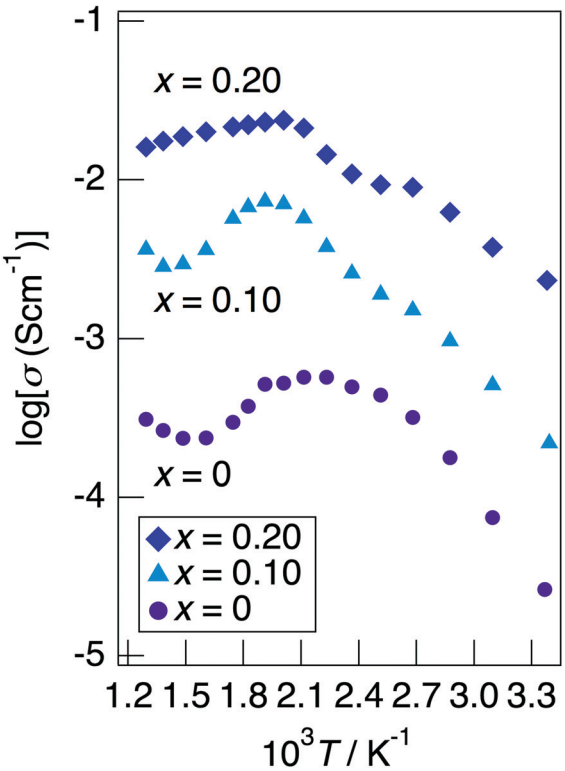

Fig. 8 The temperature dependence of the proton conductivity of $NaMg_{1-x}Li_xH_x(PO_3)_3{\cdot}yH_2O$ measured under a non-humidified N_2 gas flow.

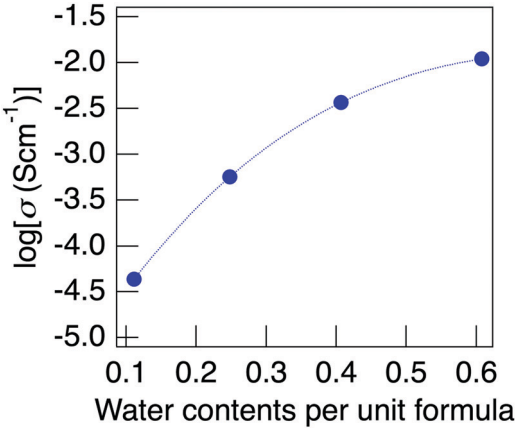

Fig. 9 The change in the proton conductivity for the water content of $NaMg_{0.8}Li_{0.2}H_{0.2}(PO_3)_3{\cdot}yH_2O$, measured at 150 °C under a non-humidified atmosphere.

with the temperature from room temperature to 125 °C, then less increase in conductivity with temperature was observed at 150 °C, at which point the second stage dehydration reaction occurred.

It decreased from 200 to 300 °C as the dehydration reaction progressed and then increased again above 300 °C. The change in conductivity for the temperature of the sample with $x = 0.10$ exhibited an intermediate behaviour between $x = 0$ and $x = 0.20$. The sample with $x = 0.20$ exhibited a high proton conductivity of 2.3×10^{-3} S cm^{-1} at 23 °C, and the highest conductivity value of 2.4×10^{-2} S cm^{-1} was obtained. The apparent activation energy of $x = 0.20$ in the range of 23–225 °C was 13.6 kJ mol^{-1}. This sample exhibited a value of over 10^{-2} S cm^{-1} in a wide temperature range of 150–500 °C. It is thought that the conductivity of the sample with $x = 0$ improves for temperature because the amount of water of crystallisation becomes almost constant at 300–600 °C, whereas the conductivity of the sample with $x = 0.20$ decreases gradually due to the desorption of water of crystallisation.

Fig. 9 presents the change in proton conductivity for the water content of $NaMg_{0.8}Li_{0.2}H_{0.2}(PO_3)_3{\cdot}yH_2O$, measured at 150 °C under a non-humidified atmosphere. Samples with low water contents were obtained by heating to a high temperature in the impedance measurement cell under a non-humidified atmosphere. The water content at the increased temperature calculated based on the TG curve was used as the water content of the sample. The conductivity of the sample containing almost no water of crystallisation was below the lower limit of measurement of the apparatus. The conductivity of $NaMg_{0.8}Li_{0.2}H_{0.2}(PO_3)_3{\cdot}yH_2O$ showed a positive tendency for the water content, which suggests proton diffusion associated with the water of crystallisation. Unlike protons, the diffusion of Na^+ and Li^+ needs the formation of defects at normal positions and the movement of interstitial sites for diffusion in the crystal structure. Since Li^+ partially occupies the Mg sites, it requires the diffusion of Mg^{2+} to diffuse in the crystal. The activation energy of Mg^{2+} estimated using the soft VB programme[28] is as high as 2.4 eV, which suggests that diffusion of Li^+ hardly occurs in this structure due to the obstruction by Mg^{2+}. The energy barrier for Na^+ diffusion also shows a high value of over 0.7 eV. It is considered that the diffusion of these cations that form the framework barely occurs in this structure. Even if the diffusion of Na^+ and Li^+ contributes to the conductivity, its value is considered to be less than 4.3×10^{-5} S cm^{-1} of the sample with the lowest water content because the movement of these cations is independent of water content. Therefore, the conductivity derived from the diffusion of Na^+ and Li^+ must be lower than 4.3×10^{-5} S cm^{-1} of the sample with the lowest water content. This value is 0.4% of the sample, exhibiting a value of 1.1×10^{-2} S cm^{-1}, and the high conductivity of this material is considered to be due to proton diffusion through water molecules.

Fig. 10 shows the temperature dependence of the proton conductivity of $NaMg_{0.8}Li_{0.2}H_{0.2}(PO_3)_3{\cdot}yH_2O$ under a humidified atmosphere (p_{H_2O} = 4 kPa). At an initial heating step, the conductivity of $NaMg_{0.8}Li_{0.2}H_{0.2}(PO_3)_3{\cdot}yH_2O$ exhibited a high proton conductivity of over 10^{-3} S cm^{-1} from room temperature, and it reached 2.6×10^{-2} S cm^{-1} at 225 °C. Although the conductivity decreased slightly from 250 °C to 350 °C due to dehydration, $NaMg_{0.8}Li_{0.2}H_{0.2}(PO_3)_3{\cdot}yH_2O$ exhibited a high proton conductivity of over 2×10^{-2} S cm^{-1}. Since the desorption of water of crystallisation is relieved under a humidified

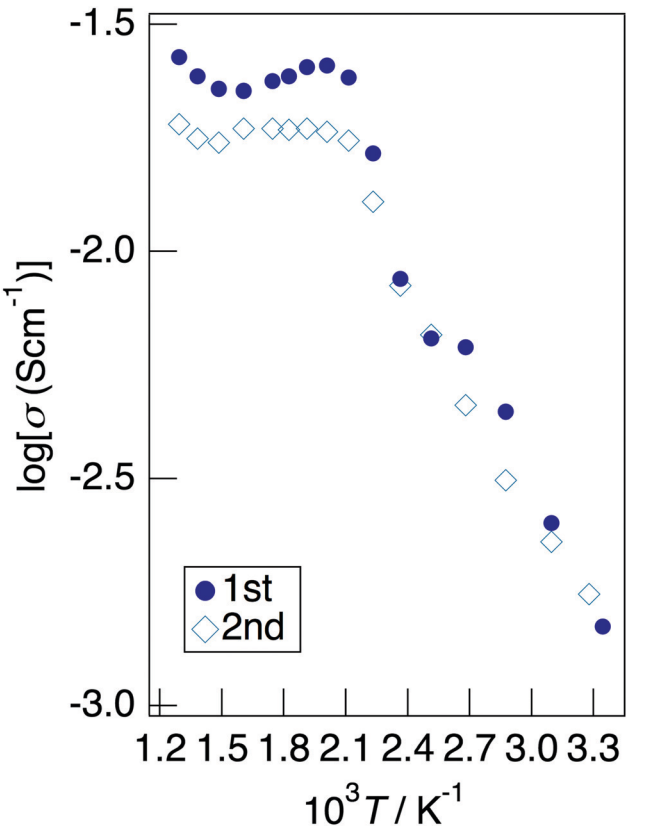

Fig. 10 The temperature dependence of the proton conductivity of $NaMg_{0.8}Li_{0.2}H_{0.2}(PO_3)_3{\cdot}yH_2O$ under a humidified atmosphere (p_{H_2O} = 4 kPa). The measurement at the second heating step was performed after holding the sample used for the initial measurement under an N_2 gas flow saturated at room temperature (p_{H_2O} = 4 kPa) for 2 h.

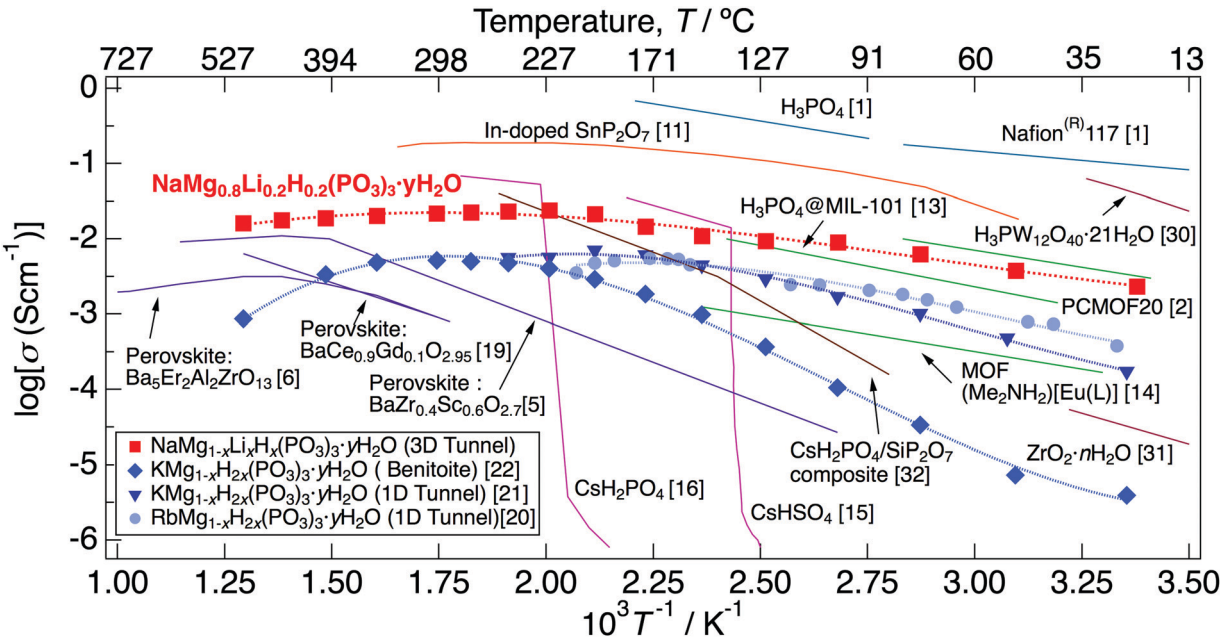

Fig. 11 The temperature dependence of the proton conductivity of $NaMg_{0.8}Li_{0.2}H_{0.2}(PO_3)_3{\cdot}yH_2O$ together with those of previously reported proton conductors.

atmosphere rather than under a non-humidified atmosphere, the conductivity would increase again above 350 °C. After the first heating step, the sample was held for 2 h in an N_2 gas flow saturated at room temperature, and then the conductivity was measured again. $NaMg_{0.8}Li_{0.2}H_{0.2}(PO_3)_3{\cdot}yH_2O$ showed a proton conductivity of over 10^{-3} S cm^{-1} from room temperature, and the value reached 1.8×10^{-2} S cm^{-1} at 225 °C in the second heating step. The sample held for 2 h at room temperature under a humidified atmosphere contained water molecules of 1.0 H_2O that was calculated from the weight loss of 30–800 °C on the TG curve, which is over 80% of the water of crystallization of the sample before the initial heating step. Since desorption and absorption of water of crystallization occur reversibly in this structure, it is considered that the high proton conductivity corresponding to the amount of water of crystallization is exhibited again under a humidified atmosphere.

Fig. 11 presents the temperature dependence of the proton conductivity of $NaMg_{0.8}Li_{0.2}H_{0.2}(PO_3)_3{\cdot}yH_2O$ together with those of previously reported proton conductors. $NaMg_{0.8}Li_{0.2}H_{0.2}(PO_3)_3{\cdot}yH_2O$ exhibits high proton conductivity over a wide temperature range from room temperature to 500 °C, and the values exceed 10^{-2} S cm^{-1} in the range of 150–500 °C. Materials impregnated with liquids, such as Nafion membranes, exhibit high proton conductivity at low temperatures with a large amount of humidification.[1] However, it is difficult to maintain high proton conductivity up to the intermediate temperature due to water volatilisation. Inorganic solids containing water molecules and polyoxometalates also exhibit high proton conductivity at low temperatures.[30,31] Many MOF materials, which have a non-combustible inorganic block and a hydrogen bond network of molecules that provide a proton diffusion pathway, exhibit a high proton conductivity below 150 °C.[2,13,14] Solid acids such as $CsHSO_4$ and CsH_2PO_4 exhibit high proton conductivity above the temperature at which the phase transition occurs.[15,16] The structure of MOF-based materials and these solid acids become thermally unstable because of the dissociation of hydrogen bonds, contrary to showing fast proton diffusion in the low-intermediate temperature range. Inorganic solid acids expand the temperature range in which high proton conductivity is exhibited as composites with other ceramics.[32] In-doped SnP_2O_7 exhibits a high proton conductivity up to 350 °C[11]; however, the conductivity has changed by five orders of magnitude by synthesis methods and research, which has caused controversy over whether the origin of proton diffusion is intercrystalline or a grain boundary.[29,33–36] Perovskites with rigid frameworks formed by only ionic/covalent bonds show excellent thermal stability and exhibit high proton conductivity at around 400 °C by the material design based on the point defects chemistry. However, an achievement of fast proton diffusion *via* the Grotthouss mechanism below 300 °C is still difficult due to the high charge density on the surface of protons.[5,6]

The three-dimensional tunnel framework of $NaMg_{0.8}Li_{0.2}H_{0.2}(PO_3)_3{\cdot}yH_2O$ is formed by the connection of (NaO_6) (MgO_6) octahedral chains and PO_4 tetrahedral chains without hydrogen bonding with water molecules. The rigid framework connected by only covalent/ionic bonds of $NaMg_{0.8}Li_{0.2}H_{0.2}(PO_3)_3{\cdot}yH_2O$ results in thermal stability up to 800 °C. Since the framework is formed without water molecules, the structure is maintained even if the dehydration reaction occurs. Because the framework was retained after dehydration at a high temperature, it exhibited high proton conductivity again after incorporating water of crystallisation. Mixed cation phosphates, $AMg_{1-x}H_{2x}(PO_3)_3{\cdot}yH_2O$ (A: K^+ and Rb^+), have water molecule chains that provide a proton diffusion pathway in a one-dimensional tunnel framework formed by $(AO_6)(MgO_6)$

octahedral chains and PO_4 tetrahedral chains and exhibit high proton conductivity from room temperature to 250 °C.[20,21] Although these phosphates have a rigid framework as well as $NaMg_{0.8}Li_{0.2}H_{0.2}(PO_3)_3{\cdot}yH_2O$, this change to the high-temperature phase allows longer distances between the A^-site cation and Mg^{2+}. Benitoite-type phosphate, which is the high-temperature phase of the 1D tunnel-type $KMg_{1-x}H_{2x}(PO_3)_3{\cdot}yH_2O$, also shows thermal stability and exhibits high proton conductivity up to 500 °C.[22] Due to the smaller cation size of Na^+ compared to K^+ and Rb^+, $NaMg_{0.8}Li_{0.2}H_{0.2}(PO_3)_3{\cdot}yH_2O$ would maintain enough distance between Na^+ and Mg^{2+} in the octahedral chain and no phase transition occurs up to the melting point. $NaMg_{0.8}Li_{0.2}H_{0.2}(PO_3)_3{\cdot}yH_2O$ exhibited higher proton conductivity over a wider temperature range than other mixed cation phosphates.

The conductivity change for the water content suggests the proton diffusion associated with the water of crystallisation in $NaMg_{0.8}Li_{0.2}H_{0.2}(PO_3)_3{\cdot}yH_2O$. In the three-dimensional tunnel framework of $NaMg_{0.8}Li_{0.2}H_{0.2}(PO_3)_3{\cdot}yH_2O$, oxygen sites of water molecules were confirmed. The connection of PO_4 tetrahedra and H_2O/H_3O^+ *via* hydrogen bonds is observed from the FTIR spectra. The connection of PO_4 tetrahedra induces the adjacent hopping sites of water molecules in the tunnel framework of mixed cation phosphates.[20,21] A part of the water molecules in $NaMg_{0.8}Li_{0.2}H_{0.2}(PO_3)_3{\cdot}yH_2O$ is coordinated to Na^+ that forms the framework. The large cation in the mixed cation phosphates tends to form coordination bonding with the oxygen of water molecules, and it enhances the retention ability of water molecules in the structure due to the stronger connection than that of the hydrogen bonds.[21] The strong connection of water molecules by the coordination bond causes a slightly lower proton conductivity of $NaMg_{0.8}Li_{0.2}H_{0.2}(PO_3)_3{\cdot}yH_2O$ at low temperatures than other water-contained systems; however, the adjacent arrangement of water molecules in the tunnel framework should result in high proton conductivity over 10^{-3} S cm^{-1} from room temperature. The increase in conductivity reached a plateau at around 200 °C due to the desorption of water of crystallisation; however, it exhibited a high proton conductivity of over 10^{-2} S cm^{-1} up to 500 °C due to the retention of water molecules by the strong connection with the rigid framework.

Conclusions

Mixed cation phosphate, $NaMg_{1-x}Li_xH_x(PO_3)_3{\cdot}yH_2O$, with a three-dimensional open framework was investigated as a fast proton conductor. $NaMg_{0.8}Li_{0.2}H_{0.2}(PO_3)_3{\cdot}yH_2O$ was synthesised by the coprecipitation method. A solid solution was formed in the composition range of x = 0–0.20. From the thermal measurement, a stepwise elimination reaction of water of crystallisation was observed. In FTIR measurements, an increase in absorption peaks corresponding to the modes of O–H and P–O–H bonds for the composition change in $NaMg_{1-x}Li_xH_x(PO_3)_3{\cdot}yH_2O$ was observed. The three-dimensional tunnel framework of $NaMg_{0.8}Li_{0.2}H_{0.2}(PO_3)_3{\cdot}yH_2O$ was formed by the connection of $(NaO_6)(MgO_6)$ octahedral chains and PO_4 tetrahedral chains. In the three-dimensional tunnel framework of $NaMg_{0.8}Li_{0.2}H_{0.2}(PO_3)_3{\cdot}yH_2O$, the oxygen sites of water molecules were confirmed. A multi-step weight loss due to desorption of water of crystallisation was observed for the TG curves. The framework was retained up to 800 °C. The proton conductivity improved with increasing x and $NaMg_{0.8}Li_{0.2}H_{0.2}(PO_3)_3{\cdot}yH_2O$ exhibited a high proton conductivity of over 10^{-2} S cm^{-1} in the temperature range of 150–500 °C, and the value reached 2.4×10^{-2} S cm^{-1} at 225 °C under a non-humidified atmosphere. The proton conductivity of $NaMg_{0.8}Li_{0.2}H_{0.2}(PO_3)_3{\cdot}yH_2O$ depends on the amount of crystalline water. Under a humidified atmosphere (p_{H_2O} = 4 kPa), $NaMg_{0.8}Li_{0.2}H_{0.2}(PO_3)_3{\cdot}yH_2O$ exhibited a conductivity of over 10^{-3} S cm^{-1} from room temperature to 500 °C and reached 2.6×10^{-2} S cm^{-1} at 225 °C. After keeping the dehydrated sample in the humidified atmosphere at room temperature for 2 h, $NaMg_{0.8}Li_{0.2}H_{0.2}(PO_3)_3{\cdot}yH_2O$ showed a proton conductivity of over 10^{-2} S cm^{-1} again in the intermediate temperature range.

Author contributions

Y. M. conceived and designed the experiments. N. U., J. N. and A. T. prepared the samples and carried out XRD and impedance measurements. N. U. carried out FTIR measurements. Y. M. and N. U. performed TG/DTA measurements. N. U. and Y. M. refined the crystal structure. Y. M., D. M., S. T., N. I., and S. H. discussed the results and analysed the data. Y. M. and N. U. wrote the manuscript.

Conflicts of interest

There are no conflicts to declare.

Acknowledgements

This work was partially supported by JSPS KAKENHI Grant Number 19H05793 for D. M. and 21K05246 for Y. M.

Notes and references

1 K. D. Kreuer, Proton Conductivity: Materials and Applications, *Chem. Mater.*, 1996, **8**, 610–641.
2 P. Ramaswamy, N. E. Wong, B. S. Gelfand and G. K. H. Shimizu, A Water Stable Magnesium MOF that Conducts Protons over 10^{-2} S cm^{-1}, *J. Am. Chem. Soc.*, 2015, **137**, 7640–7643.
3 I. Baranov, V. P. Khiznichenko, V. A. Sandler and L. A. Shuvalov, Frequency Dielectric Dispersion in the Ferroelectric and Superionic Phases of CsH_2PO_4, *Ferroelectrics*, 1988, **81**, 183–186.
4 M. Nagao, T. Kamiya, P. Heo, A. Tomita, T. Hibino and M. Sano, Proton Conduction in In^{3+}-Doped SnP_2O_7 at Intermediate Temperatures, *J. Electrochem. Soc.*, 2006, **153**, A1604–A1609.

5 J. Hyodo, K. Kitabayashi, K. Hoshino, Y. Okuyama and Y. Yamazaki, Fast and Stable Proton Conduction in Heavily Scandium-Doped Polycrystalline Barium Zirconate at Intermediate Temperatures, *Adv. Energy Mater.*, 2020, **10**, 200213.
6 T. Murakami, J. R. Hester and M. Yashima, High Proton Conductivity in $Ba_5Er_2Al_2ZrO_{13}$, a Hexagonal Perovskite-Related Oxide with Intrinsically Oxygen-Deficient Layers, *J. Am. Chem. Soc.*, 2020, **142**, 11653–11657.
7 H. Luecke, B. Schobert, H. T. Richter, J. P. Cartailler and J. K. Lanyi, Structural Changes in Bacteriorhodopsin During Ion Transport at 2 Angstrom Resolution, *Science*, 1999, **286**, 255–260.
8 W. Gu and V. Helms, Tightly Connected Water Wires Facilitate Fast Proton Uptake at the Proton Entrance of Proton Pumping Proteins, *J. Am. Chem. Soc.*, 2009, **131**, 2080–2081.
9 S. Iwata, C. Ostermeier, B. Ludwig and H. Michel, Structure at 2.8 Å Resolution of Cytochrome *c* Oxidase from Paracoccus Denitrificans, *Nature*, 1995, **376**, 660–669.
10 D. A. Boysen, T. Uda, C. R. I. Chisholm and S. M. Haile, High-Performance Solid Acid Fuel Cells Through Humidity Stabilization, *Science*, 2004, **303**, 68–70.
11 T. Hibino, Intermediate-Temperature Proton Conductors and their Applications to Energy and Environmental Devices, *J. Ceram. Soc. Jpn.*, 2011, **119**, 677–686.
12 M. Inukai, S. Horike, T. Itakura, R. Shinozaki, N. Ogiwara, D. Umeyama, S. Nagarkar, Y. Nishiyama, M. Malon, A. Hayashi, T. Ohhara, R. Kiyanagi and S. Kitagawa, Encapsulating Mobile Proton Carriers into Structural Defects in Coordination Polymer Crystals: High Anhydrous Proton Conduction and Fuel Cell Application, *J. Am. Chem. Soc.*, 2016, **138**, 8505–8511.
13 V. G. Ponomareva, K. A. Kovalenko, A. P. Chupakhin, D. N. Dybtsev, E. S. Shutova and V. P. Fedin, Imparting High Proton Conductivity to a Metal–Organic Framework Material by Controlled Acid Impregnation, *J. Am. Chem. Soc.*, 2012, **134**, 15640–15643.
14 Y. S. Wei, X. P. Hu and Z. Han, X, Y, Dong, S. Q. Zang and T. C. W. Mak, Unique Proton Dynamics in an Efficient MOF-Based Proton Conductor, *J. Am. Chem. Soc.*, 2017, **139**, 3505–3512.
15 A. I. Baranov, L. A. Shuvalov and N. M. Schagina, Superion Conductivity and Phase Transitions in $CsHSO_4$ and $CsHSeO_4$ crystals, *JETP Lett.*, 1982, **36**, 459–462.
16 S. M. Haile, C. R. I. Chisholm, K. Sasaki, D. A. Boysen and T. Uda, Solid Acid Proton Conductors: From Laboratory Curiosities to Fuel Cell Electrolytes, *Faraday Discuss.*, 2007, **134**, 17–39.
17 A. I. Baranov, V. P. Khiznichenko, V. A. Sandler and L. A. Shuvalov, Frequency Dielectric Dispersion in the Ferroelectric and Superionic Phases of CsH_2PO_4, *Ferroelectrics*, 1988, **81**, 183–186.
18 H. Iwahara, T. Esaka, H. Uchida and N. Maeda, Proton Conduction in Sintered Oxides and its Application to Steam Electrolysis for Hydrogen Production, *Solid State Ionics*, 1981, **3–4**, 359–363.
19 N. Bonanos, B. Ellis, K. S. Knight and M. N. Mahmood, Ionic Conductivity of Gadolinium-doped Barium Cerate Perovskites, *Solid State Ionics*, 1989, **35**, 179–188.
20 Y. Matsuda, M. Yonemura, H. Koga, C. Pitteloud, M. Nagao, M. Hirayama and R. Kanno, Synthesis, crystal structure, and ionic conductivity of tunnel structure phosphates, $RbMg_{1-x}H_{2x}(PO_3)_3{\cdot}y(H_2O)$, *J. Mater. Chem. A*, 2013, **1**, 15544–15551.
21 Y. Matsuda, K. Funakoshi, R. Sebe, G. Kobayashi, M. Yonemura, N. Imanishi, D. Mori and S. Higashimoto, Arrangement of Water Molecules and High Proton Conductivity of Tunnel Structure Phosphates, $KMg_{1-x}H_{2x}(PO_3)_3{\cdot}yH_2O$, *RSC Adv.*, 2020, **10**, 7803–7811.
22 Y. Matsuda, N. Ueda, K. Funakoshi, J. Nakajima, D. Mori, S. Taminato and S. Higashimoto, Proton Conductivity in Mixed Phosphate, $KMg_{1-x}H_{2x}(PO_3)_3{\cdot}yH_2O$ with a Layered Structure at Low-Intermediate Temperatures, *Dalton Trans.*, 2021, **50**, 7678–7685.
23 A. A. Kapshuk, P. G. Nagorny and O. V. Petrenko, Synthesis, IR Spectra, and Structures of Double Metaphosphates, $MNi(PO_3)_3$ (M = Na or K), *Crystallogr. Rep.*, 2000, **45**(2), 206–209.
24 A. Rene, D. Rene, D. Andre, P. Marie Therese and Q. D. Tran, Preparation and Crystallographic Study of $KM(PO_3)_3$ Type Trimetaphosphates, *C. R. Seances Acad. Sci., Ser. B*, 1966, **262**(B(10)), 718–721.
25 A. Maierhaba, P. Xiaobo, H. Shujuan, R. Yilimiranmu, Y. Zhihua, W. Hongping and P. Shilie, $MIMIIP_3O_9$ (MI = Rb, MII = Cd, Mg, Ca; MI = Cs, MII = Pb, Sr; MI = K, MII = Mg): Cation Substitution Application in Cyclophosphate Family and Nonlinear Optical Properties, *Inorg. Chem.*, 2018, **57**, 7372–7379.
26 I. Abrahams, A. Ahmed, C. J. Groombridge, G. E. Hawkes and T. G. Nunes, Cation Distribution in Cubic $NaM(PO_3)_3$ (M = Mg or Zn) Using X-ray Powder Diffraction and Solid State NMR, *J. Chem. Soc., Dalton Trans.*, 2000, **24**, 4479–4701.
27 R. Oishi, M. Yonemura, Y. Nishimaki, S. Torii, A. Hoshikawa, T. Ishigaki, T. Morishima, K. Mori and T. Kamiyama, Rietveld Analysis Software for J-PARC, *Nucl. Instrum. Methods Phys. Res., Sect. A*, 2009, **600**, 94–96.
28 H. Chen, L. L. Wong and S. Adams, SoftBV—A software tool for screening the materials genome of inorganic fast ion conductors, *Acta Crystallogr.*, 2019, **B75**, 18–33.
29 C. R. Kreller, H. H. Pham, M. S. Wilson, R. Mukundan, N. Henson, M. Sykora, M. Hartl, L. Daemen and F. H. Garzon, Intragranular Phase Proton Conduction in Crystalline $Sn_{1-x}In_xP_2O_7$ (x = 0 and 0.1), *Phys. Chem. C*, 2017, **121**(43), 23896–23905.
30 A. Hardwick, P. G. Dickens and R. C. T. Slade, Investigation of H+ Motion in the 21-Hydrates of 12-Tungstophosphoric and 12-Molybdophosphoric Acids by AC Conductivity and Pulsed ^{1}H NMR Measurements, *Solid State Ionics*, 1984, **13**, 345–350.
31 W. A. England, M. G. Cross, A. Hamnett, P. J. Wisemam and J. B. Goodenough, Fast Proton Conduction in Inorganic Ion Exchange Compounds, *Solid State Ionics*, 1980, **1**, 231–249.
32 V. Ponomareva and G. Lavrova, Controlling the Proton Transport Properties of Solid Acids *via* Structural and Microstructural Modification, *J. Solid State Chem.*, 2011, **15**, 213–221.

33 S. R. Phadke, C. R. Bowers, E. D. Wachsman and J. C. Nino, Proton Conduction in Acceptor Doped SnP_2O_7, *Solid State Ionics*, 2011, **183**, 26–31.
34 S. Tao, Conductivity of SnP_2O_7 and In-Doped SnP_2O_7 Prepared by an Aqueous Solution Method, *Solid State Ionics*, 2009, **180**, 148–153.
35 X. Xu, S. Tao, P. Wormald and J. T. S. Irvine, Intermediate Temperature Stable Proton Conductors Based Upon SnP_2O_7, Including Additional H_3PO_4, *J. Mater. Chem.*, 2010, **20**, 7827–7833.
36 H. Wang, J. Xiao, Z. Zhou, F. Zhang, H. Zhang and G. Ma, Ionic Conduction in Undoped SnP_2O_7 at Intermediate Temperatures, *Solid State Ionics*, 2010, **181**, 1521–1524.